Under low-pressure conditions ($<10^{-3}$ mbar), the sample temperature remained constant, unaffected by variations of the surface composition and reactivity. Such patterns have previously been modeled theoretically by appropriate reaction-diffusion equations (*4*, *5*). However, when the pressure was increased by more than two orders of magnitude (into the pressure range not accessible by PEEM), the situation changed markedly. Because of the higher turnover rate, the sample temperature was considerably affected by the released heat of reaction. For the gas composition with the highest turnover, the increase in temperature was as high as 40 K at a total pressure of 0.5 mbar. When the CO/O_2 partial pressure ratio was further increased, the surface changed from the reactive into the less reactive state, associated with a rapid decrease of the sample temperature. To reestablish a high reaction rate, we had to intermediately lower p_{CO}. The resulting transient state is reflected in EMSI images (Fig. 3). At t = 2 s, an O-rich spiral wave appeared. This spiral propagated into the CO-covered region, such that after 3 s, roughly half of the imaged surface area was in the reactive O-rich state. Because of the increase of reactivity, the sample temperature rose, which further enhanced the decrease of the CO concentration by desorption, such that after about 3.2 s, the whole surface was in the predominantly O-covered and highly reactive state—that is, had turned bright. The speed of the reaction front was determined from the video frames between the last two images of Fig. 3 to be about 5 mm/s.

We have been able to observe pattern formation and propagating reaction fronts up to total pressures of 1 atm. Limitations at even higher pressures were encountered because the UHV chamber used in the experiments is unsuitable for such conditions.

A previously unseen type of pattern was found (Fig. 4) at $p_{O_2} = 2.22 \times 10^{-2}$ mbar. Its features are reminiscent of target patterns known from pure reaction-diffusion behavior at lower pressures (*4*). However, while the latter are periodically emitted from fixed trigger centers (presumably surface defects) and propagate continuously, the present patterns appear at random, like raindrops on a flat water surface rapidly dying out after a short propagation length. This behavior may be described by the superposition of reaction-diffusion and thermokinetic effects. The pronounced damping of wave propagation and the role of nonisothermal effects in this system will have to be analyzed in the future by detailed theoretical modeling.

The rather simple optical methods EMSI and RAM presented here allowed the investigation of pattern formation associated with heterogeneously catalyzed reactions from UHV up to atmospheric pressures. An upper pressure limit for the applicability of these methods is not apparent. In addition, with the spatial resolution principally limited by diffraction, these methods will enable the study of other surface processes occurring at length scales from the submicrometer up to several millimeters, and the present temporal resolution of 20 ms can certainly be improved significantly.

REFERENCES AND NOTES

1. P. Stoltze and J. K. Nørskov, *Phys. Rev. Lett.* **55**, 2502 (1985).
2. M. Eiswirth and G. Ertl, in *Chemical Waves and Patterns*, K. Showalter and R. Kapral, Eds. (Kluwer, Amsterdam, 1995), p. 447.
3. H. H. Rotermund, W. Engel, M. Kordesch, G. Ertl, *Nature* **343**, 355 (1990).
4. G. Ertl, *Science* **254**, 1750 (1991).
5. M. Bär, S. Nettesheim, H. H. Rotermund, M. Eiswirth, G. Ertl, *Phys. Rev. Lett.* **74**, 1246 (1995).
6. V. V. Barelko, I. I. Kurachka, A. G. Merzhanav, K. G. Shkadinskii, *Chem. Eng. Sci.* **33**, 805 (1978); S. L. Lane and D. Luss, *Phys. Rev. Lett.* **70**, 830 (1993); F. Quin, E. E. Wolf, A. C. Chang, *ibid.* **72**, 1459 (1994).
7. R. Reiter, H. Motschmann, H. Orendi, A. Nemetz, W. Knoll, *Langmuir* **8**, 1784(1992); R. F. Cohn, J. W. Wagner, J. Kruger, *Appl. Opt.* **27**, 4664 (1988).
8. J. J. Carroll, T. E. Madey, A. J. Melmed, D. R. Sandstrom, *Surf. Sci.* **96**, 508 (1980).
9. D. A. Woolf *et al.*, *Phys. Rev. B* **51**, 4691 (1995).
10. S. Jakubith, H. H. Rotermund, W. Engel, A. von Oertzen, G. Ertl, *Phys. Rev. Lett.* **65**, 3013 (1990).

11. We acknowledge B. E. Argyle and W. Schrittenlacher for numerous useful suggestions and illuminating discussions.

4 August 1995; accepted 20 September 1995

Nanoscale Complexity of Phospholipid Monolayers Investigated by Near-Field Scanning Optical Microscopy

Jeeseong Hwang,* Lukas K. Tamm, Christine Böhm, Tirunelveli S. Ramalingam, Eric Betzig,† Michael Edidin

Near-field scanning optical microscopy of phospholipid monolayers doped with fluorescent lipid analogs reveals previously undescribed features in various phases, including a concentration gradient at the liquid-expanded/liquid-condensed domain boundary and weblike structures in the solid-condensed phase. Presumably, the web structures are grain boundaries between crystalline solid lipid. These structures are strongly modulated by the addition of low concentrations of cholesterol and ganglioside G_{M1} in the monolayer.

Lipid monolayers have been used to study two-dimensional systems, to construct organized arrays and matrices, and to model biological membranes (*1*). An understanding of their structure is critical to all of these efforts. At the molecular level, much has been learned from x-ray and electron diffraction (*2*), scanning tunneling microscopy (STM), and atomic force microscopy (AFM) (*3*). It is also possible to analyze lipid monolayers on a larger scale by far-field epifluorescence microscopy (FFM) (*4*–*7*) of monolayers doped with fluorescent lipid analogs. Such studies have shown that, in the fluid-solid coexistence region, lipid monolayers exhibit domain structures. The size and shape of these domains vary with temperature, pressure, and the chemical composition of the monolayer. In particular, low concentrations of certain compounds (such as cholesterol) alter the line tension at the boundary between two coexisting phases, thereby changing the domain

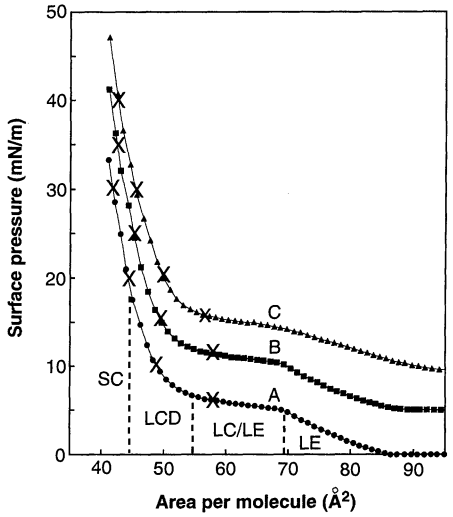

Fig. 1. The πA isotherms of (curve A) DPPC/0.5 mol % Bodipy-PC, (curve B) DPPC/0.5 mol % Bodipy-PC/1 mol % cholesterol, and (curve C) DPPC/0.5 mol % Bodipy-PC/0.5 mol % ganglioside G_{M1} monolayers at the air-water interface. For clarity, isotherms B and C are shifted upward with an offset of +5 and +10 mN/m, respectively, in surface pressure. Four different regions (LE, LE/LC, LCD, and SC) corresponding to different lipid phases are distinguished. Points at which the monolayers were sampled are marked by X's on the curves.

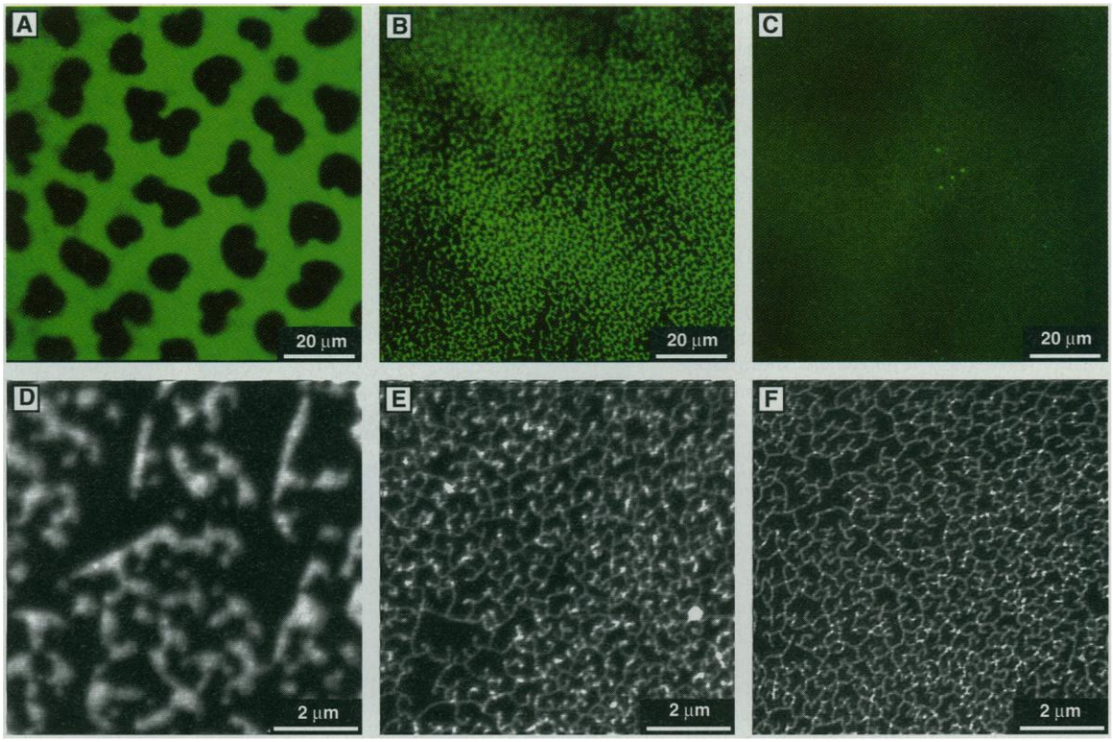

Fig. 2. (**A** through **C**) FFM images of DPPC/0.5 mol % Bodipy-PC monolayers sampled at three different pressures: (A) 7 mN/m, (B) 10 mN/m, and (C) 30 mN/m. (**D** through **F**) NSOM images of the same monolayers sampled at three different surface pressures: (D) 10 mN/m, (E) 20 mN/m, and (F) 30 mN/m. The web structure in (E) and (F) could reflect the presence of nanoscale crystals with hexagonally packed lipids, as observed by x-ray and electron diffraction from transferred and nontransferred lipid monolayers (*2*).

structure. This behavior has been the focus of several theoretical treatments (*4*).

Little is known about lipid monolayer structures at a scale between 10 nm and 1 μm. This has been largely the result of a lack of techniques operating in this range. Although AFM is able to disclose structures at this scale, it is limited to studying changes in the surface topology or, in rare cases, changes in the rheology of thin films. A more promising approach is to use near-field scanning optical microscopy (NSOM) (*8*, *9*). This technique combines the fluorescence contrast of conventional optics with spatial resolution as fine as 30 to 50 nm. Here we take advantage of these features to investigate the structure of lipid monolayers transferred from an air-water interface to a glass substrate under controlled surface pressure (*10*, *11*). The samples were first imaged by NSOM and then by FFM (*12*).

Pressure-area (πA) isotherms were obtained for samples of the following: (i) 99.5 mol % 1,2-dipalmitoyl-sn-glycero-3-phosphocholine (DPPC)/0.5 mol % Bodipy-PC, (ii) DPPC/0.5 mol % Bodipy-PC/1 mol %

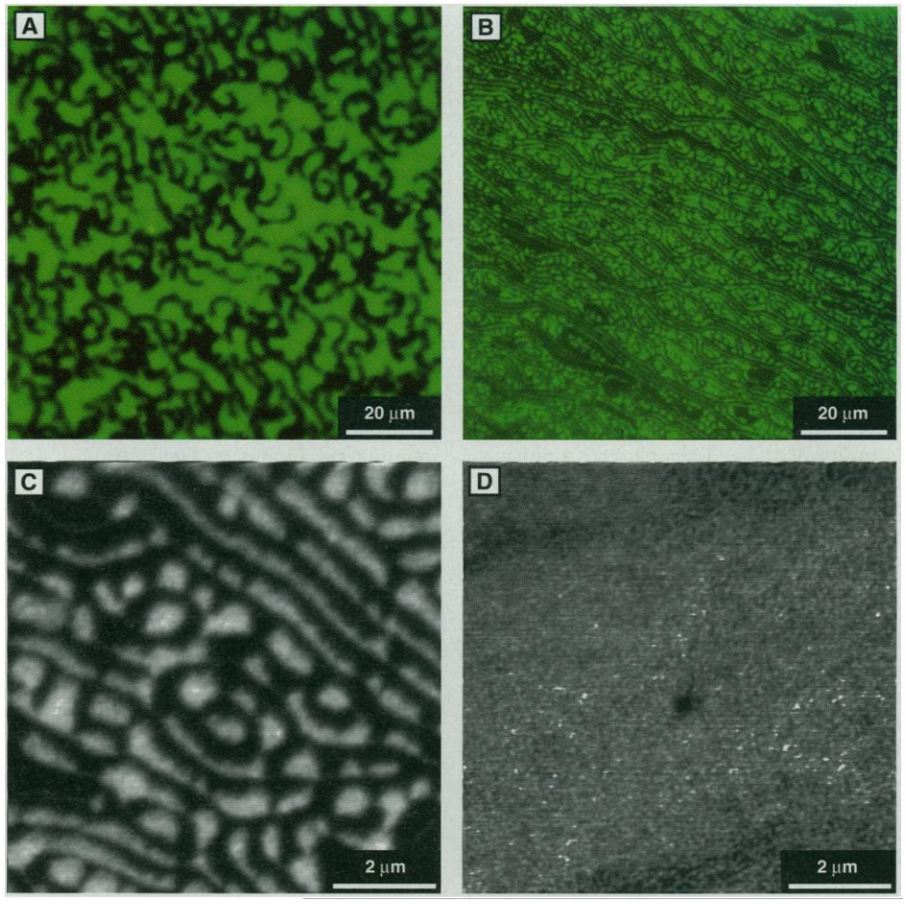

Fig. 3. FFM images of DPPC/Bodipy-PC/1.0 mol % cholesterol monolayers sampled at (**A**) 7 mN/m and (**B**) 10 mN/m. (**C**) NSOM images of the same monolayers transferred at 10 mN/m and (**D**) 20mN/m (*20*).

J. Hwang, T. S. Ramalingam, M. Edidin, Department of Biology, The Johns Hopkins University, Baltimore, MD 21218, USA.
L. K. Tamm and C. Böhm, Department of Molecular Physiology and Biological Physics, University of Virginia, Charlottesville, VA 22908, USA.
E. Betzig, AT&T Bell Laboratories, Murray Hill, NJ 07974, USA.

*To whom correspondence should be addressed.
†Present address: NSOM Enterprises, Berkeley Heights, NJ 07922, USA.

cholesterol, and (iii) DPPC/0.5 mol % Bodipy-PC/0.5 mol % ganglioside G_{M1} (Fig. 1). Four different regions corresponding to different lipid phases can be distinguished in the πA curves: (i) a liquid-expanded (LE) phase, (ii) a region of coexistence of LE and liquid-condensed (LC) phases, (iii) a LC-dominant (LCD) phase, and (iv) a solid-condensed (SC) phase.

Our FFM images of the DPPC/Bodipy-PC monolayer showed features of a single-component phospholipid monolayer phase transition (Fig. 2, A through C). Similar results have been reported for monolayers that were doped with other fluorescent probes that partition favorably into the LE phase within the LE/LC coexistence region (*5*, *6*, *11*). As the monolayer was compressed from the LE into the LE/LC coexistence region, small LC domains, which exclude Bodipy-PC, arose at various locations and then gradually grew in size. Some domains showed chiral features, as previously observed in similar systems (*13*). The sample transferred at pressure π = 10 mN/m exhibited a mottled structure with many fluorescent domains surrounded by a dark background (Fig. 2B). Frequently, these structures were too fine to be resolved by FFM. At even higher pressure, the samples were featureless as observed by FFM (Fig. 2C). In contrast, NSOM resolved many previously undescribed structural details, including uneven distribution of fluorescent molecules in the LE domains, gradual domain boundaries between the LE and LC regions (Fig. 2D), and a fine web structure with frequent intersections of ~120° (Fig. 2, E and F).

Low concentrations, 1 mol %, of cholesterol in DPPC monolayers changed the morphology of these lipid domains. In the region of LE/LC coexistence, cholesterol reduced the line tension energy between domains, so that long thin LC domains were formed (Fig. 3A). The shape and chirality of these domains were similar to those observed by FFM in nitrobenzoxadiazole-labeled phosphocholine (NBD-PC)/(*R*)-DPPC/cholesterol monolayers (*7*). As the surface pressure was increased to 10 mN/m, the domains further thinned and elongated (Fig. 3B). The NSOM images at the same pressure showed that the larger LE domains were connected by thin strings of LE lipid, which are too narrow and dim to be detected by FFM (Fig. 3C). Even though these strings have not been detected previously, their existence is consistent with current theories that suggest they arise in the presence of cholesterol from a reduction of the line tension energy, which opposes the dipolar energy of the LC domains (*4*, *7*). At higher pressure, NSOM images showed a compact web structure, which became more dense as the pressure was further increased (Fig. 3D).

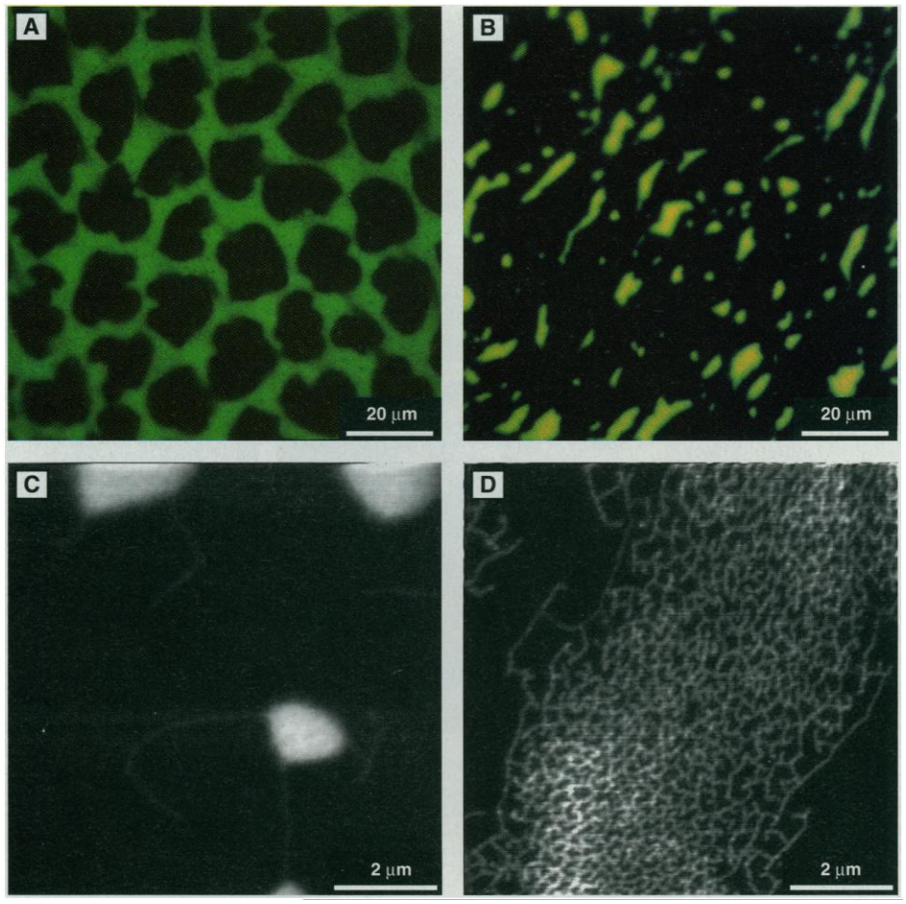

Fig. 4. FFM images of DPPC/Bodipy-PC/0.5 mol % ganglioside G_{M1} monolayers transferred at (**A**) 7 mN/m and (**B**) 10 mN/m. (**C**) NSOM images of the same monolayers transferred at 10 mN/m and (**D**) 20 mN/m.

Addition of 0.5 mol % of the ganglioside G_{M1} to the DPPC monolayer also had significant effects on the formation and structure of membrane domains. The dark LC domains that developed as the monolayer was compressed were faceted, grew to larger size than in the undoped DPPC/Bodipy-PC monolayers (compare Figs. 2A and 4A), and merged together, leaving residual LE phase domains between them (Fig. 4B). At 10 mN/m, the concentration of Bodipy-PC in these remaining LE domains was so high that the fluorescence spectrum shifted from green to yellow, as described elsewhere for Bodipy-PC in cell membranes (*14*). The corresponding NSOM image at 10 mN/m revealed fluorescent, thin "whiskers" stretching out from these bright domains (Fig. 4C). These whiskers may represent residual LE domains between LC domains that did not coalesce completely because of residual G_{M1} that remained trapped at the grain boundaries. At higher G_{M1} concentrations, 1 mol %, all domains were interconnected by whiskers. Thus, these interstitial regions likely represent domains of G_{M1} in the LE phase that are separated from domains of DPPC in the LC phase. As the pressure was increased to 20 mN/m, each fluorescent patch was again broken into a web structure whose density increased with pressure (Fig. 4D).

Besides resolving additional features in lipid monolayers, NSOM permits quantitative measurement of domain boundaries, monolayer composition, and the partition of the Bodipy-PC probe into the various phases. For example, NSOM showed that the fluorescence intensity gradually diminishes across the LE/LC domain boundary (Fig. 5), rather than exhibiting the sharp discontinuity of a simple phase boundary. This gradient can be explained in terms of a recent electrostatic model that demonstrates electric fields, near critical points, can induce concentration gradients in monolayers even without phase separation (*15*). According to this model, the concentration gradient depends on several parameters—such as the electric field gradient, molecular packing densities, and the dipole densities of lipid components—and is expected to change in response to variations in these experimentally controllable parameters. In fact, in

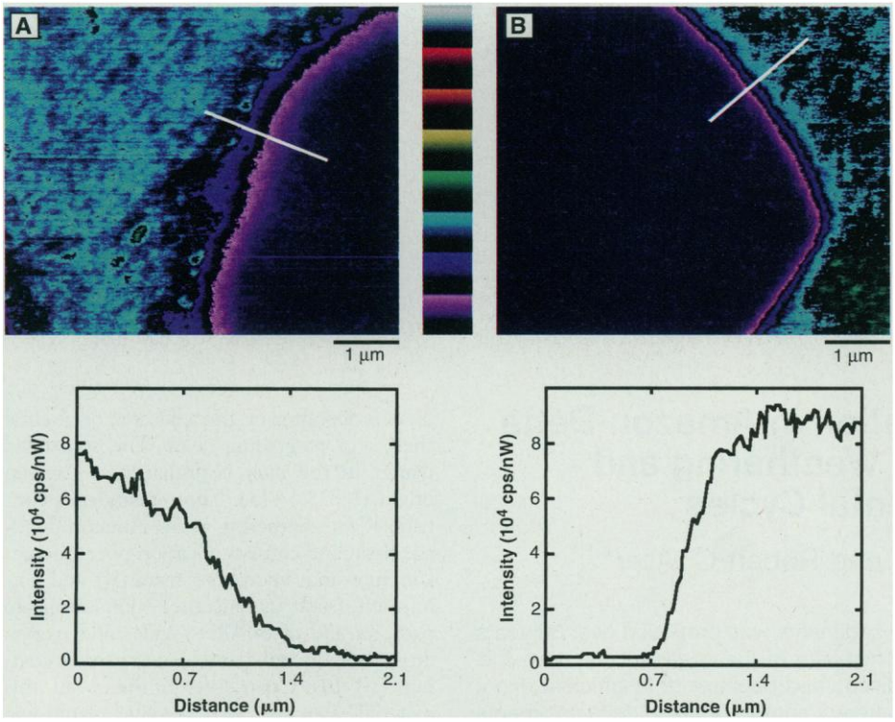

Fig. 5. Concentration gradient of Bodipy-PC molecules across the LE/LC domain boundary of $\pi = 7$ mN/m samples. (**A**) An NSOM image of the domain boundary region of a DPPC/Bodipy-PC sample and the intensity profile along the line. (**B**) An NSOM image and the intensity profile of a DPPC/0.5 mol % Bodipy-PC/0.5 mol % ganglioside G_{M1} sample. The signal intensity is normalized for the excitation power from the NSOM probe.

monolayers containing 0.5 mol % G_{M1} the gradient was steeper than in monolayers with only Bodipy-PC probe in DPPC (Fig. 5B). This gradient suggests that addition of G_{M1} molecules with negatively charged head groups alter these parameters either by screening dipole moments or by changing the molecular packing densities. We also found that the fluorescence-intensity gradient became steeper as the surface pressure of the monolayer was increased (*16*). This behavior is expected if the dipole moment of the Bodipy moiety is decreased when the long axis of Bodipy molecule is aligned perpendicular to the subphase surface as the packing density of the lipids increases.

Earlier work on the fluorescence imaging of single molecules with NSOM (*17*) provided a calibration of the instrument that allowed us to extract information on the monolayer composition and probe partitioning from histograms of the observed fluorescence intensities. Given the quantum yield of Bodipy-PC and an aperture radius of ~40 nm, we determined number densities in the LE phase of $\sim 5.8 \times 10^3$ and $\sim 1.3 \times 10^4$ Bodipy-PC molecules per square micrometer at pressures of 4 and 7 mN/m, respectively. These values are consistent with those calculated from the mole fraction of Bodipy-PC, the molecular area determined from the πA curve, and the fractional area of the LE phase as measured from FFM images (*18*).

The same analysis at higher pressures showed that during the transition from LCD to SC phase, Bodipy-PC probes are forced into the SC phase. The minimum intensity measured for the SC phase in samples at 20 mN/m corresponded to ~220 molecules/μm^2, shifting to ~760 molecules/μm^2 as the pressure increased to 30 mN/m. This analysis implies that at high pressures the SC phase is not completely free of fluorescent probe, even though Bodipy-PC partitions strongly into the less condensed phase. Intensity distributions measured for G_{M1}-containing monolayers demonstrated lower densities, ~60 and ~340 Bodipy-PC molecules/μm^2 at 20 and 30 mN/m, respectively, thereby indicating that G_{M1} suppresses the movement of Bodipy-PC molecules from the less condensed to the more condensed regions of the monolayer.

The high resolution and molecular sensitivity of NSOM might be used to study other issues involving lipid monolayers in addition to those discussed above. For example, the orientations of single molecules incorporated into domains of different phases could be measured to study tilt angles and molecular packing, and simultaneous fluorescent labeling for lipids and incorporated proteins could be used in the study of lipid-protein interactions and domain formation in model and cell membranes (*19*).

REFERENCES AND NOTES

1. H. M. McConnell, T. H. Watts, R. M. Weis, A. A. Brian, *Biochim. Biophys. Acta* **864**, 95 (1986); P. Hinterdorfer, G. Baber, L. K. Tamm, *J. Biol. Chem.* **269**, 20360 (1994).
2. J. M. Mikrut, P. Dutta, J. B. Ketterson, R. C. MacDonald, *Phys. Rev. B* **48**, 14479 (1993); C. Böhm, H. Möhwald, L. Leiserowitz, J. Als-Nielsen, K. Kjaer, *Biophys. J.* **64**, 553 (1993); A. Fisher and E. Sackmann, *J. Phys. Paris* **45**, 517 (1984).
3. A. L. Weisenhorn *et al.*, *Langmuir* **7**, 8 (1991); J. Garnaes, D. K. Schwartz, R. Viswanathan, J. A. N. Zasadzinski, *Nature* **357**, 54 (1992); L. F. Chi, M. Anders, H. Fuchs, R. R. Johnston, H. Ringsdorf, *Science* **259**, 213 (1993); J. Yang *et al.*, *J. Microscopy* **171**, 183 (1993).
4. H. M. McConnell, *Annu. Rev. Phys. Chem.* **42**, 171 (1991); H. Möhwald, *ibid.* **41**, 441 (1990).
5. M. Lösche, E. Sackmann, H. Möhwald, *Ber. Bunsenges. Phys. Chem.* **87**, 848 (1983); R. Peters and K. Beck, *Proc. Natl. Acad. Sci. U.S.A.* **80**, 7183 (1983).
6. H. M. McConnell, L. K. Tamm, R. M. Weis, *Proc. Natl. Acad. Sci. U.S.A.* **81**, 3249 (1984).
7. R. M. Weis and H. M. McConnell, *J. Phys. Chem.* **89**, 4453 (1985); W. M. Heckl, D. A. Cadenhead, H. Möhwald, *Langmuir* **4**, 1352 (1988).
8. E. Betzig and J. K. Trautman, *Science* **257**, 189 (1992).
9. M. H. P. Moers, H. E. Gaub, N. F. van Hulst, *Langmuir* **10**, 2774 (1994).
10. We formed lipid monolayers at 21° ± 5°C by spreading a freshly prepared mixture of 99.5 mol % DPPC (Avanti Polar Lipids) and 0.5 mol % of the fluorescent lipid analog Bodipy-PC (Molecular Probes, D-3803) in chloroform-ethanol solution, at the air-water (Milli-Q, pH 5.5) interface of a Langmuir-Blodgett trough (NIMA, Coventry, UK) equipped with a Wilhelmy balance to measure the surface pressure of the monolayer. After allowing the solvent to evaporate for several minutes, the monolayer was compressed at a speed of 41 mm^2/s with pauses at different surface pressures to transfer samples of monolayer to glass substrates. Details of the method are described in L. K. Tamm, *Biochemistry* **27**, 1450 (1988). The FFM images showed that the acyl chain–labeled Bodipy-PC has the same partition behavior in the LE/LC coexistence region as does NBD-PC (Molecular Probes, N-3787).
11. The transfer procedure does not appear to greatly disturb the morphologies of the monolayers on the length scale of our interest. Previous epifluorescence, electron, and surface plasmon microscopy studies showed, at various length scales, only small distortions of monolayers transferred onto hydrophilic glass substrates [(*6*); M. Seul, S. Subramanian, H. M. McConnell, *J. Phys. Chem.* **89**, 3592 (1985); A. Fischer, M. Lösche, H. Möhwald, E. Sackmann, *J. Phys. Paris Lett.* **45**, 785 (1984); W. Hickel and W. Knoll, *J. Appl. Phys.* **67**, 3572 (1990)]. In our work the transferred areas of the monolayers agreed with the calculated areas of the substrates. Sequential FFM micrographs of transferred monolayers in the LE/LC coexistence region also showed the same domain shapes as those seen by FFM of monolayers before transfer.
12. Details of the NSOM setup are described in (*8, 17*). The FFM observations were made with a ×100, 1.3–numerical aperture objective.
13. R. M. Weis and H. M. McConnell, *Nature* **310**, 47 (1984).
14. R. E. Pagano, O. C. Martin, H. C. Kang, R. P. Haugland, *J. Cell Biol.* **113**, 1267 (1991).
15. K. Y. C. Lee, J. F. Klingler, H. M. McConnell, *Science* **263**, 655 (1994). Zwitterionic lipids such as DPPC and Bodipy-PC have different dipole densities in the LC and LE domains; an electric field gradient is created as a result of the excess dipole moment in the LC domain. The molecular composition of the LE domains can be treated as a binary

mixture of DPPC and Bodipy-PC molecules under the influence of the electric field, resulting in the concentration gradient of Bodipy-PC in LE domains near the boundary of LC domains. Even though the monolayers were sampled only from compression cycles and were not compared with the samples from expansion cycles, we believe that the partition of fluorescent molecules had reached equilibrium at the moment of transfer. The interval between compression and transfer (several minutes) was enough time for the distribution of fluorescent molecules to reach equilibrium through diffusion. The diffusion coefficient of DPPC in the LE domain is 10^{-7} to 10^{-8} cm^2/s.
16. Averaged half-decay lengths (the lateral distances where the fluorescent intensities fall to half those of the maxima) determined from the cursor profiles across the domain boundaries for the monolayers sampled at π = 7, 10, 20, and 30 mN/m were 661 ± 133, 181 ± 38, 65 ± 15, and 37 ± 8 nm, respectively, in DPPC/Bodipy-PC samples and 345 ± 31, 143 ± 33, 57 ± 17, and 56 ± 13 nm, respectively, in the samples with an additional 0.5 mol % of ganglioside G_{M1}.
17. E. Betzig and R. J. Chichester, *Science* **262**, 1422 (1993).
18. The peak signal from a single lipophilic carbocyanine dye, dil-C_{18}(3) (Molecular Probes, D-282), molecule in a transferred DPPC monolayer was ~250 counts per second (cps) per nanowatt of tip power, which is ~20% of the typical value for a single molecule embedded in polymethylmethacrylate (*17*). This implies a quantum yield of ~0.2 for a Bodipy in the monolayer, resulting in the equivalent emission signal of 1200 cps/nW. In DPPC/Bodipy-PC samples, average intensities of the LE phase are ~35,000 cps/nW at π = 4 mN/m and ~75,000 cps/nW at π = 7 mN/m. The calculated number densities of the dye molecules in this phase are ~7.4×10^3 and ~1.3×10^4 molecules/μm^2, respectively.
19. J. Hwang, E. Betzig, M. Edidin, R. J. Chichester, *Biophys. J.* **66**, A277 (1994).
20. Dark spots at the center were caused by the dwell of the probe at one spot during the characterization of the near-field signal before scanning began.
21. We thank R. Chichester and R. Pagano for their valuable help and suggestions and H. McConnell for helpful discussions. Supported by NIH grants AI14584, DK44375 (M.E.), and AI30557 (L.K.T.).

8 June 1995; accepted 10 August 1995

Rapid Clay Mineral Formation in Amazon Delta Sediments: Reverse Weathering and Oceanic Elemental Cycles

Panagiotis Michalopoulos and Robert C. Aller*

Formation of aluminosilicate minerals in marine sediments was proposed over 30 years ago as a potentially important control on the chemistry of the oceans. Until now, this reverse weathering process has been largely discounted because of insufficient direct evidence for its existence. Experiments with unaltered, anoxic, Amazon delta sediments showed that substantial quantities of K-Fe-Mg clay minerals precipitated on naturally occurring solid substrates over times of ~12 to 36 months at ~28°C. A range of pore-water, solute-flux, and solid-phase criteria indicates that comparable clay mineral precipitation processes occur throughout Amazon shelf sediments, contributing ≥3 percent of the weight of the deposits and consuming ~10 percent of the global riverine K^+ flux.

The rapid formation of authigenic clay minerals during early sedimentary diagenesis was originally hypothesized as a likely process substantially influencing oceanic chemistry and closing a variety of elemental cycles through reverse weathering (*1*). The concept has not gained wide acceptance because of the lack of direct evidence for precipitation of such minerals in major deltas. Discovery of massive hydrothermal cycling of elements at midocean ridges has also decreased the obvious necessity for sedimentary sinks for certain solutes in geochemical budgets (*2*). However, problems concerning the geochemical balance of several major and minor elements still exist and can be overcome if early diagenetic formation of aluminosilicate minerals is assumed (*3*).

Authigenic glauconitic green clays form in small but concentrated amounts in continental shelf sands, upwelling areas, and sedimentary microenvironments, but such clays are usually considered relict, forming over thousands of years (*4*). Low-temperature authigenic smectites are also known to form from siliceous biogenic debris and metal oxides in local regions influenced by hydrothermal metal sources (*5*). Evidence for clay formation in nearshore depositional environments with high sediment accumulation rates has been indirect and has usually been inferred from observed trends in pore water solutes (K, F, Mg, and Al) or from small changes in solid-phase elemental compositions and operational leaches (*6–8*). In these latter cases, transported debris dominates accumulated material and makes documentation of disseminated authigenic clays difficult. In a few cases, direct evidence for nearshore early diagenetic clay formation (for example, the presence of nontronite, illite-smectite, and berthierine) has been found (*9*, *10*). The presence of authigenic clays documented to date in a range of environments therefore makes it certain that such minerals can form under the right conditions. The major questions that remain are whether the formation of such phases is rapid and whether it is geochemically significant.

As part of a general study of diagenetic processes in Amazon delta sediments, we investigated the potential formation of authigenic minerals during deposition (*11*). The Amazon River contributes ~6% of the total river particulates delivered annually to the oceans (*12*). Most of the Amazon river sediment is deposited on the adjacent continental shelf as a prograding delta. The suspended matter in the river is primarily of Andean origin (~82%) (*13*). The remainder is contributed by weathering in the Amazon drainage basin and consists of cation-poor (such as kaolinite and amorphous material) and cation-rich (such as smectite) aluminosilicate particles and of Si,Al,Fe oxides and oxyhydroxides as discrete particles and particle coatings (*10*, *14*). Upon entering the ocean, this material is mixed with reactive planktonic debris (organic carbon and SiO_2) and undergoes a variety of diagenetic changes, including extensive mobilization of Fe and Mn (*15*).

We simulated the conditions under which authigenic mineral precipitation must take place in a series of sediment incubation experiments that allowed ready separation of reaction products from the sedimentary matrix. To do this, we inserted small quantities (~0.5 g) of well-characterized solid substrates directly into otherwise unaltered Amazon delta sediments. Sediment was collected from the upper ~1 to 2 m of both inshore and offshore delta sites by means of box and kasten-type gravity corers. Except for possible diffusive exchange with overlying water or physical reworking by currents, material was subsequently maintained under conditions typical of burial in the delta. Substrates were (i) standard kaolinite, representative of the cation-poor aluminosilicate material that is one product of the tropical weathering regime of the Amazon basin; (ii) quartz sand grains, also a typical transported sediment component; (iii) FeOOH-coated quartz grains, representative of lateritic debris and commonly present in these sediments; and (iv) glass beads, simulating amorphous silica diatom frustrules, a biogenic product of photosynthesis in the water column that is deposited in Amazon delta sediments (*16*). Each substrate type was attached by a thin film of epoxy onto an acrylic slide, covered with a 0.4-μm nuclepore membrane filter and a nylon mesh outer screen, and inserted into the center of 250- to 1000-ml plastic bottles filled with natural Amazon delta sediment (wet and unaltered). Bottles were

Marine Sciences Research Center, State University of New York, Stony Brook, NY 11794–5000, USA.

*To whom correspondence should be addressed.